Physica D 331 (2016) 48–57

Contents lists available at ScienceDirect

Physica D

journal homepage: www.elsevier.com/locate/physd

Nonlinear wave dynamics near phase transition in $\mathcal{PT}$-symmetric localized potentials

Sean Nixon, Jianke Yang *

Department of Mathematics and Statistics, University of Vermont, Burlington, VT 05401, United States

HIGHLIGHTS

- Analysis for the NLS equation with a $\mathcal{PT}$-symmetric potential is presented.
- A $\mathcal{PT}$-Krein theory is developed for phase transition in this $\mathcal{PT}$-symmetric system.
- Nonlinear dynamics near phase transition is derived analytically.
- Comparison with numerics shows good agreement.

ARTICLE INFO

Article history:
Received 15 June 2015
Received in revised form
12 April 2016
Accepted 13 May 2016
Available online 24 May 2016
Communicated by Peter David Miller

Keywords:
$\mathcal{PT}$-symmetric systems
Nonlinear Schrödinger equation
Phase transition

ABSTRACT

Nonlinear wave propagation in parity-time symmetric localized potentials is investigated analytically near a phase-transition point where a pair of real eigenvalues of the potential coalesce and bifurcate into the complex plane. Necessary conditions for a phase transition to occur are derived based on a generalization of the Krein signature. Using the multi-scale perturbation analysis, a reduced nonlinear ordinary differential equation (ODE) is derived for the amplitude of localized solutions near phase transition. Above the phase transition, this ODE predicts a family of stable solitons not bifurcating from linear (infinitesimal) modes under a certain sign of nonlinearity. In addition, it predicts periodically-oscillating nonlinear modes away from solitons. Under the opposite sign of nonlinearity, it predicts unbounded growth of solutions. Below the phase transition, solution dynamics is predicted as well. All analytical results are compared to direct computations of the full system and good agreement is observed.
© 2016 Elsevier B.V. All rights reserved.

1. Introduction

Parity-time ($\mathcal{PT}$) symmetric systems started out from an observation in non-Hermitian quantum mechanics, where a complex but $\mathcal{PT}$-symmetric potential could possess all-real spectrum [1]. This concept later spread out to optics, Bose–Einstein condensation, mechanical systems, electric circuits and many other fields, where a judicious balancing of gain and loss constitutes a $\mathcal{PT}$-symmetric system which can admit all-real linear spectrum [2–16]. For example, in optics, an even refractive index profile together with an odd gain–loss landscape yields a $\mathcal{PT}$-symmetric system. A common phenomenon in linear $\mathcal{PT}$-symmetric systems is the existence of a phase transition (also known as $\mathcal{PT}$-symmetry breaking), where pairs of real eigenvalues collide and then bifurcate to the complex plane when the magnitude of gain and loss is above a certain threshold [1,7,17–19]. This phase transition has been observed experimentally in a wide range of physical systems [4–6,8,13,14]. When nonlinearity is present in $\mathcal{PT}$ systems, the interplay between nonlinearity and $\mathcal{PT}$ symmetry gives rise to additional novel properties such as the existence of continuous families of stationary nonlinear modes, stabilization of nonlinear modes above phase transition, and symmetry breaking of nonlinear modes [7,18–28]. These findings reveal that $\mathcal{PT}$-symmetric systems break the boundary between traditional conservative and dissipative systems and open new exciting research territories. Practical applications of $\mathcal{PT}$ systems are emerging as well, such as recent demonstrations of $\mathcal{PT}$-symmetric micro-ring lasers and unidirectional reflectionless $\mathcal{PT}$ metamaterials [12,15,16].

Phase transition is an important property of linear $\mathcal{PT}$-symmetric systems which is at the heart of many proposed applications [12,16,29]. At a phase transition, a pair of real eigenvalues coalesce and form an exceptional point featuring a non-diagonal Jordan block (i.e., the algebraic multiplicity of the eigenvalue is higher than the geometric multiplicity). In the presence of nonlinearity (such as when the wave amplitude is not small), the interplay between the phase transition and nonlinearity is a fascinating

* Corresponding author.
E-mail address: jyang@math.uvm.edu (J. Yang).

http://dx.doi.org/10.1016/j.physd.2016.05.006
0167-2789/© 2016 Elsevier B.V. All rights reserved.

subject. This interplay was previously studied for periodic $\mathcal{PT}$-symmetric potentials in [25,30,31], where novel behaviors such as wave-blowup and temporally-oscillating bound states were reported below phase transition. In addition, stable nonlinear Bloch modes were reported above phase transition because nonlinearity transforms the effective potential from above to below phase transition [25] (a similar phenomenon was reported in [32] for a different $\mathcal{PT}$-symmetric dimer model). However, in periodic potentials above phase transition, the presence of unstable infinitely extended linear modes makes the zero background unstable everywhere, which excludes the possibility of stable spatially-localized coherent structures. In localized potentials, will the situation be different?

In this article we study nonlinear wave behaviors in localized $\mathcal{PT}$-symmetric potentials near a phase transition. Unlike periodic potentials, the instability of linear modes above phase transition is limited to the area around the localized potential. In this case, the addition of nonlinearity can balance against the effects of gain and loss making stable spatially-localized coherent structures, such as solitons and oscillating bound states, possible above phase transition. Mathematically, we explain this phenomenon by a multi-scale perturbation analysis, where a reduced nonlinear ordinary differential equation (ODE) is derived for the amplitude of localized solutions near phase transition. Above phase transition, this ODE model predicts a family of stable solitons not bifurcating from linear (infinitesimal) modes under a certain sign of nonlinearity. In addition, it predicts persistent oscillating nonlinear modes away from solitons. Under the opposite sign of nonlinearity, it predicts unbounded growth of solutions. Similarly, solution dynamics below phase transition is predicted as well. All these predictions are verified in the full partial differential equation (PDE) system. In addition to these nonlinear dynamics, we also derive a necessary condition for a phase transition to occur at an exceptional point in the linear $\mathcal{PT}$ system by a generalization of the Krein signature, namely, a phase transition from a collision of two real eigenvalues is possible only when the two eigenvalues have opposite $\mathcal{PT}$-Krein signatures.

2. Preliminaries

The mathematical model we consider in this article is the following potential NLS equation

$$\mathrm{i}\psi_z + \psi_{xx} + V(x;\epsilon)\psi + \sigma|\psi|^2\psi = 0, \tag{2.1}$$

where $V(x;\epsilon)$ is a $\mathcal{PT}$-symmetric complex potential, i.e.,

$$V^*(-x;\epsilon) = V(x;\epsilon), \tag{2.2}$$

parameterized by ϵ, $\sigma = \pm 1$ is the sign of nonlinearity, and the superscript * represents complex conjugation. Throughout the text, we assume that the potential $V(x;\epsilon)$ is continuous with ϵ. Eq. (2.1) governs nonlinear light propagation in an optical medium with gain and loss [18] as well as the dynamics of Bose–Einstein condensates in a double-well potential with atoms injected into one well and removed from the other well [9,10]. $\mathcal{PT}$-symmetric optical systems have been realized experimentally [5,6,12,14–16], however $\mathcal{PT}$-symmetric Bose–Einstein condensates remain theoretical. Without loss of generality, we assume a phase transition occurs at $\epsilon = 0$, where a pair of real eigenvalues of the potential coalesce and form an exceptional point, whose algebraic multiplicity is two and the geometric multiplicity is one. We will analyze the solution dynamics in Eq. (2.1) near this exceptional point, i.e., when $|\epsilon| \ll 1$.

The analysis to be developed applies to all localized $\mathcal{PT}$-symmetric potentials near a phase transition. To illustrate these analytical results and compare them with direct numerics of the full model (2.1), we will use a concrete example—the so-called Scarff II potential

$$V = V_R\,\mathrm{sech}^2(x) + \mathrm{i}W_0\,\mathrm{sech}(x)\tanh(x), \tag{2.3}$$

where V_R and W_0 are real parameters. For this potential, phase transition occurs at $W_0 = V_R + 1/4$ [17], and solitons as well as robust oscillating solutions have been reported numerically below phase transition in [18,33–35].

3. $\mathcal{PT}$-Krein signature and a necessary condition for phase transition

For the potential NLS equation (2.1), when one looks for linear eigenmodes $\psi = u(x)\mathrm{e}^{-\mathrm{i}\mu z}$, with regards to the stability of the zero state, the eigenvalue problem

$$L(x;\epsilon)u = -\mu u \tag{3.1}$$

will be obtained, where

$$L = \partial_{xx} + V(x;\epsilon) \tag{3.2}$$

is a Schrödinger operator with a complex $\mathcal{PT}$-symmetric potential, and μ is an eigenvalue. We wish to consider the phase-transition process by which the spectrum of L changes from all-real to partially-complex. This phase transition occurs when a pair of real eigenvalues collide, forming an exceptional point, and then bifurcate into the complex plane. It is important to recognize that not any two real eigenvalues can turn complex upon collision. This is analogous to the linear stability of equilibria in Hamiltonian systems, where not just any two purely imaginary eigenvalues upon collision can bifurcate off the imaginary axis and result in linear instability [36–39]. With this in mind, we consider the question: under what conditions can a pair of real eigenvalues of L induce a phase transition upon collision?

We will work in the square-integrable doubly-differentiable Hilbert functional space H^2 endowed with the standard inner product

$$\langle f, g\rangle = \int_{-\infty}^{\infty} f^*(x)g(x)\,dx.$$

Under this inner product, the adjoint operator $L^\dagger$ of L is

$$L^\dagger = L^* = \partial_{xx} + V^*(x;\epsilon).$$

When the potential $V(x)$ is $\mathcal{PT}$-symmetric, a key property of the operator L, which can be readily verified, is

$$L^\dagger = \mathcal{P}L\,\mathcal{P}^{-1}, \tag{3.3}$$

where $\mathcal{P}$ is the parity operator, i.e., $\mathcal{P}f(x) \equiv f(-x)$. For this parity operator, $\mathcal{P}^{-1} = \mathcal{P}$ and $\mathcal{P}^\dagger = \mathcal{P}$, thus $\mathcal{P}$ is Hermitian and invertible. Consequently, L is pseudo-Hermitian [40] and $\mathcal{P}L$ is Hermitian.

One of the consequences of the pseudo-Hermiticity of L is that, any complex eigenvalues of L must come in conjugate pairs (μ, μ^*). The reason is that under pseudo-Hermiticity, $L^\dagger$ is similar to L, thus $L^\dagger$ and L share the same spectrum. But the spectrum of $L^\dagger$ is the complex conjugate of L's, thus complex eigenvalues of L must come in (μ, μ^*) pairs.

Another consequence of the pseudo-Hermiticity of L is that, it allows us to define a $\mathcal{PT}$-Krein signature for discrete real eigenvalues of L, which will prove to be important when studying phase transition from collisions of L's real eigenvalues. For this purpose, we endow the Hilbert space H^2 with another indefinite $\mathcal{PT}$ inner product [41]

$$\langle f, g\rangle_{\mathcal{PT}} \equiv \langle f, \mathcal{P}g\rangle = \int_{-\infty}^{\infty} f^*(x)g(-x)\,dx. \tag{3.4}$$

Since $\mathcal{P}$ is Hermitian, this $\mathcal{PT}$-product naturally satisfies the symmetry condition

$$\langle g, f\rangle_{\mathcal{PT}} = \langle f, g\rangle^*_{\mathcal{PT}}. \tag{3.5}$$

Thus, for any complex function $f(x)$, $\langle f, f\rangle_{\mathcal{PT}}$ is real. In addition, $\langle f, f\rangle_{\mathcal{PT}}$ is independent of the overall phase of f since it is invariant under $f(x) \rightarrow f(x)e^{i\theta}$, where θ is a phase constant. More importantly, under this $\mathcal{PT}$-product, the operator L is symmetric, i.e.,

$$\langle Lf, g\rangle_{\mathcal{PT}} = \langle f, Lg\rangle_{\mathcal{PT}}, \tag{3.6}$$

the reason being

$$\langle Lf, g\rangle_{\mathcal{PT}} = \langle Lf, \mathcal{P}g\rangle = \langle f, L^\dagger \mathcal{P}g\rangle = \langle f, \mathcal{P}Lg\rangle = \langle f, Lg\rangle_{\mathcal{PT}}$$

by virtue of the pseudo-Hermitian property of L. This symmetric property of L will be convenient for us to prove certain orthogonality relations between L's eigenfunctions in later text of this section.

For an eigenmode $[\mu, u(x)]$ of L with a simple real eigenvalue μ we define its $\mathcal{PT}$-Krein signature as

$$\mathrm{S}_\mu = \mathrm{sgn}\left[\langle u, u\rangle_{\mathcal{PT}}\right]. \tag{3.7}$$

Note that $\langle u, u\rangle_{\mathcal{PT}}$ is always real in view of the symmetry property (3.5). In addition, $\langle u, u\rangle_{\mathcal{PT}} \neq 0$. The reason is that for a simple eigenvalue μ of L, the generalized-eigenfunction equation

$$(L + \mu)u_g = u \tag{3.8}$$

cannot admit a solution in the Hilbert space. Due to the pseudo-Hermitian property of L, when $(L + \mu)u = 0$, $(L + \mu)^\dagger(\mathcal{P}u) = 0$, thus $\mathcal{P}u$ is in the kernel of the adjoint operator of $L + \mu$. So the Fredholm condition for Eq. (3.8) to not admit a solution is

$$\langle u, \mathcal{P}u\rangle = \langle u, u\rangle_{\mathcal{PT}} \neq 0. \tag{3.9}$$

Because of this, the $\mathcal{PT}$-Krein signature of a simple real eigenvalue is always positive or negative. In addition, this signature cannot change under a continuous variation of the parameter ϵ unless pairs of such eigenvalues collide. The reason is that this change of signature can only occur through $\langle u, u\rangle_{\mathcal{PT}} = 0$, which cannot happen as long as μ remains a simple real eigenvalue, see Eq. (3.9).

It is helpful to compare this $\mathcal{PT}$-Krein signature with the regular Hamiltonian–Krein signature for linearized Hamiltonian systems. Such a system takes the form $J\mathcal{L}u = \lambda u$, where $\mathcal{L}$ is Hermitian and J invertible and anti-Hermitian. The Hamiltonian–Krein signature for a simple imaginary eigenvalue λ of this system is defined as $\mathrm{sgn}\left[\langle u, \mathcal{L}u\rangle\right] = \mathrm{sgn}[\langle u, \lambda J^{-1}u\rangle]$ [38]. For our eigenvalue problem (3.1), the pseudo-Hermitian property of L allows us to rewrite it as

$$(i\mathcal{P})^{-1}(\mathcal{P}L)u = (i\mu)u, \tag{3.10}$$

where $\mathcal{P}L$ is Hermitian, and $(i\mathcal{P})^{-1} = -i\mathcal{P}$ is anti-Hermitian and invertible. This eigenvalue equation is then of the same form as $J\mathcal{L}u = \lambda u$, with $\mathcal{L} = \mathcal{P}L$, $J = (i\mathcal{P})^{-1}$, and $\lambda = i\mu$. Thus, if one copies the definition of the Hamiltonian–Krein signature to the above equation, this definition would be $S_\mu = \mathrm{sgn}[-\mu\langle u, u\rangle_{\mathcal{PT}}]$, which differs from our definition (3.7) by a mere constant. For our purposes, this constant difference is unimportant.

The main result of this section is that when two simple real eigenvalues of L collide, a necessary condition for a phase transition is the two real eigenvalues have opposite $\mathcal{PT}$-Krein signatures. This result extends an analogous one in Hamiltonian systems to $\mathcal{PT}$-symmetric systems [36,38,39]. In view of the connection between our eigenvalue problem (3.10) and the Hamiltonian problem $J\mathcal{L}u = \lambda u$, this result is hardly surprising. The proof we will employ is, however, somewhat different from those in [36,38,39].

We first present three lemmas.

Lemma 3.1. *Let $u_1(x)$ and $u_2(x)$ be two eigenfunctions of the operator L with real eigenvalues μ_1 and μ_2 respectively. If $\mu_1 \neq \mu_2$, then $\langle u_1, u_2\rangle_{\mathcal{PT}} = 0$.*

Proof. Using the symmetry property (3.6) we have

$$\langle u_1, Lu_2\rangle_{\mathcal{PT}} = \langle Lu_1, u_2\rangle_{\mathcal{PT}}.$$

Then, using the fact that u_1 and u_2 are eigenfunctions, we can calculate the left and right sides of the above equation as

$$\langle u_1, Lu_2\rangle_{\mathcal{PT}} = -\mu_2\langle u_1, u_2\rangle_{\mathcal{PT}},$$

and

$$\langle Lu_1, u_2\rangle_{\mathcal{PT}} = -\mu_1\langle u_1, u_2\rangle_{\mathcal{PT}}.$$

Thus, if $\mu_1 \neq \mu_2$ then $\langle u_1, u_2\rangle_{\mathcal{PT}} = 0$. □

Lemma 3.2. *Let $u(x)$ be an eigenfunction of the operator L with a complex eigenvalue μ. Then $\langle u, u\rangle_{\mathcal{PT}} = 0$.*

Proof. From Eq. (3.6) we have $\langle u, Lu\rangle_{\mathcal{PT}} = \langle Lu, u\rangle_{\mathcal{PT}}$. Calculating the two sides of this equation we get

$$(\mu - \mu^*)\langle u, u\rangle_{\mathcal{PT}} = 0.$$

Thus, if μ is complex then $\langle u, u\rangle_{\mathcal{PT}} = 0$. □

Lemma 3.3. *Let $\{e_j\}$ be a basis for an N-dimensional functional subspace in H^2 and $f = \sum_{j=1}^N c_j e_j$. Then*

$$\langle f, f\rangle_{\mathcal{PT}} = c^H M c,$$

where M is a $N \times N$ Hermitian matrix with elements given by

$$M_{ij} = \langle e_i, e_j\rangle_{\mathcal{PT}}, \tag{3.11}$$

and the superscript H represents the Hermitian (conjugate transpose) of a vector. This matrix M will be called the dual matrix of the quadratic form $\langle f, f\rangle_{\mathcal{PT}}$ on the subspace $\{e_j\}$.

Proof. Substituting the f expression into $\langle f, f\rangle_{\mathcal{PT}}$ and utilizing the linearity of the $\mathcal{PT}$-product, this lemma can be readily proved. The Hermiticity of M comes directly from the symmetry condition (3.5). □

This leads us to the main result of this section.

Theorem 3.4. *For the operator $L(x; \epsilon)$ parameterized by ϵ, if a pair of simple real eigenvalues collide and induce a phase transition at $\epsilon = 0$, then before the phase transition the two real eigenvalues must have opposite $\mathcal{PT}$-Krein signatures.*

Proof. Let $u_1(x)$ and $u_2(x)$ be two eigenfunctions of L with eigenvalues μ_1 and μ_2 respectively. When $\epsilon < 0$, μ_1 and μ_2 are simple real with $\mu_1 \neq \mu_2$; when $\epsilon > 0$, μ_1 and μ_2 are complex with $\mu_1 = \mu_2^*$; and when $\epsilon = 0$, $\mu_1 = \mu_2$, which is a double eigenvalue with a non-diagonal Jordan block. We analyze the quadratic form $\langle f, f\rangle_{\mathcal{PT}}$ restricted to the spectral subspace $X = \mathrm{span}(u_1, u_2)$ by looking at the dual Hermitian matrix M. We will show that at $\epsilon = 0$, this M matrix is non-singular and its two real eigenvalues have opposite signs, thus the quadratic form $\langle f, f\rangle_{\mathcal{PT}}$ restricted to X is indefinite. Then, since the subspace X is continuous with ϵ, the quadratic form $\langle f, f\rangle_{\mathcal{PT}}$ on the subspace X must be indefinite as well when ϵ is in a small neighborhood of 0. For $\epsilon < 0$, this will imply that the two real eigenvalues of L have opposite $\mathcal{PT}$-Krein signatures before collision.

First we discuss the case when $\epsilon = 0$, where the two real eigenvalues of L collide and the double real eigenvalue $\mu_1 = \mu_2$ has a non-diagonal Jordan block. In this case, the spectral subspace X is

$X = \text{span}(u_1, u_g)$, where u_g is the generalized eigenfunction satisfying

$$(L + \mu_1)u_g = u_1.$$

Since $\mathcal{P}u_1$ is in the kernel of the adjoint operator of $L + \mu_1$ due to the pseudo-Hermiticity of L, the Fredholm condition on the above inhomogeneous equation yields

$$\langle u_1, u_1\rangle_{\mathcal{PT}} = 0, \tag{3.12}$$

thus

$$M_{\epsilon=0} = \begin{bmatrix} 0 & c_1 \\ c_1^* & c_2 \end{bmatrix}, \tag{3.13}$$

where $c_1 = \langle u_1, u_g\rangle_{\mathcal{PT}}$ and $c_2 = \langle u_g, u_g\rangle_{\mathcal{PT}}$. Note that $c_1 \neq 0$ since it is the Fredholm condition for the double eigenvalue μ_1 not to have a second generalized eigenfunction. Then $\det(M_{\epsilon=0}) < 0$, hence $M_{\epsilon=0}$ is non-singular with a pair of real eigenvalues of opposite sign. This means that the quadratic form $\langle f, f\rangle_{\mathcal{PT}}$ restricted to X is indefinite at $\epsilon = 0$.

Since the spectral subspace X is continuous with ϵ, by continuity the quadratic form $\langle f, f\rangle_{\mathcal{PT}}$ restricted to X must be indefinite as well when ϵ is in a small neighborhood of 0. This implies that the dual matrix M must be non-singular with two real eigenvalues of opposite sign in the same ϵ neighborhood of 0.

When $\epsilon < 0$, since μ_1 and μ_2 are strictly real, then in view of Lemma 3.1,

$$M_{\epsilon<0} = \begin{bmatrix} a_1 & 0 \\ 0 & a_2 \end{bmatrix}, \tag{3.14}$$

where $a_1 = \langle u_1, u_1\rangle_{\mathcal{PT}}$ and $a_2 = \langle u_2, u_2\rangle_{\mathcal{PT}}$. Notice that a_1 and a_2 are real and non-zero (see Eq. (3.9)), thus $M_{\epsilon<0}$ is non-singular, in agreement with the prediction of the previous paragraph. In addition, since the two eigenvalues of M must have opposite signs, a_1 and a_2 then have opposite signs, which shows that the two real eigenvalues of L have opposite $\mathcal{PT}$-Krein signatures before collision.

When $\epsilon > 0$, if μ_1 and μ_2 turn complex with $\mu_1 = \mu_2^*$ (as assumed in Theorem 3.4), then by Lemma 3.2 we see that

$$M_{\epsilon>0} = \begin{bmatrix} 0 & b \\ b^* & 0 \end{bmatrix}, \tag{3.15}$$

where $b = \langle u_1, u_2\rangle_{\mathcal{PT}}$. By virtue of the pseudo-Hermiticity of L and $\mu_2 = \mu_1^*$, we can easily verify that $(L + \mu_1)^\dagger(\mathcal{P}u_2) = 0$, thus $\mathcal{P}u_2$ is in the kernel of the adjoint operator of $L + \mu_1$. Then, since μ_1 is a simple eigenvalue of L, the generalized eigenfunction equation $(L+\mu_1)u_g = u_1$ cannot admit a solution in the Hilbert space. Thus, the Fredholm alternative indicates that $\langle u_1, \mathcal{P}u_2\rangle \neq 0$, i.e., $b \neq 0$. This means that $M_{\epsilon>0}$ is non-singular with a pair of real eigenvalues of opposite sign, in agreement with the prediction above. However, when $\epsilon > 0$, μ_1 and μ_2 do not have to turn complex—they may pass through each other and stay real (see Fig. 1 for an example). Thus, opposite $\mathcal{PT}$-Krein signatures of colliding eigenvalues are only a necessary, but not sufficient, condition for phase transition. □

Now we use an example to illustrate this theorem. In the Scarff-II potential (2.3), we fix $V_R = 5$ and vary the gain–loss coefficient W_0. The linear spectra for various W_0 values are displayed in Fig. 1. It is seen that a phase transition occurs at $W_0 = 5.25$, where a pair of simple real eigenvalues coalesce and form an exceptional point, which then turns complex when $W_0 > 5.25$. We have calculated the $\mathcal{PT}$-Krein signatures of those real eigenvalues before the phase transition, which are indicated by colors in the figure. It is seen that those signatures are indeed opposite of each other, in agreement with Theorem 3.4.

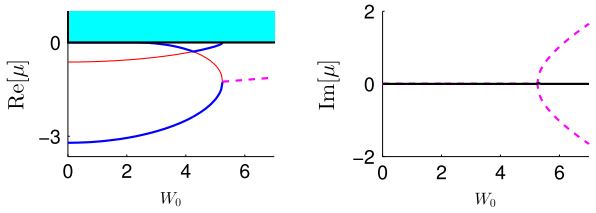

Fig. 1. Eigenvalues μ for varying gain–loss strength W_0 in the Scarff-II potential (2.3) with $V_R = 5$ (the continuous spectrum is displayed in light blue). Thick blue lines indicate eigenvalues with positive $\mathcal{PT}$-Krein signatures while thin red lines indicate eigenvalues with negative $\mathcal{PT}$-Krein signatures. Complex eigenvalues are indicated with dotted purple lines. (For interpretation of the references to color in this figure legend, the reader is referred to the web version of this article.)

Interestingly, Fig. 1 also shows another collision of simple real eigenvalues of opposite $\mathcal{PT}$-Krein signatures at $W_0 = 4.25$ (which creates another exceptional point). However, after collision these real eigenvalues re-emerge and no complex eigenvalues bifurcate out. This shows that a collision of real eigenvalues of opposite $\mathcal{PT}$-Krein signatures is a necessary but not sufficient condition for complex-eigenvalue bifurcation. A sufficient condition for complex-eigenvalue bifurcation can be found in the next section (i.e., $\alpha \neq 0$, see the paragraph below Eq. (4.10)). This condition is not met at the exceptional point of $W_0 = 4.25$ (where $\alpha = 0$), thus we do not see a phase transition there. Another interesting phenomenon at the exceptional point of $W_0 = 4.25$ in Fig. 1 is that, as W_0 passes through this exceptional point, the two real eigenvalues exchange their signatures after collision. This behavior contrasts that for a matrix-pencil example in [42], where two eigenvalues of opposite Krein signatures retain their signatures after collision.

In this section, the key property of L which allowed us to define a $\mathcal{PT}$-Krein signature for its real eigenvalues is its pseudo-Hermiticity (3.3). In general, for any pseudo-Hermitian operator L such that $L^\dagger = \eta L \eta^{-1}$, where η is a certain Hermitian operator, the complex eigenvalues of L always come in conjugate pairs (μ, μ^*). In addition, for a simple discrete real eigenvalue μ of L, we can define its η-Krein signature as $\text{sgn}[\langle u, \eta u\rangle]$, where $u(x)$ is the eigenfunction of μ. Then, if two simple real eigenvalues collide, a necessary condition for a complex-eigenvalue bifurcation is that the two real eigenvalues have opposite η-Krein signatures. The proofs for these more general statements are identical to those given in this section.

4. Reduced model near phase transition

In this section, we consider the potential nonlinear Schrödinger equation (2.1) and analyze its solution dynamics near a phase transition.

Let us suppose the $\mathcal{PT}$-symmetric potential in Eq. (2.1) takes the form

$$V(x; \epsilon) = V_0(x) + \epsilon^2 V_2(x), \tag{4.1}$$

where $0 < \epsilon \ll 1$. Here $V_0(x)$ is the unperturbed potential, $V_2(x)$ is the form of potential perturbation, and ϵ^2 is the strength of this perturbation. We assume that the unperturbed potential $V_0(x)$ is at a phase transition and possesses an exceptional point at $\mu = \mu_0$, i.e., the linear operator $\partial_{xx} + V_0(x)$ has a single eigenfunction $u_e(x)$ and a generalized eigenfunction $u_g(x)$ at μ_0. Defining

$$L_0 \equiv \partial_{xx} + V_0(x) + \mu_0, \tag{4.2}$$

we have

$$L_0 u_e = 0, \qquad L_0 u_g = u_e. \tag{4.3}$$

In addition, from Eq. (3.12) we see that $\langle u_e, u_e\rangle_{\mathcal{PT}} = 0$.

In principle, an exceptional point can have algebraic multiplicities higher than two, meaning that it can have additional generalized eigenfunctions beside u_g. But in a generic case, an exceptional point is formed by the collision of two simple real eigenvalues, in which case its algebraic multiplicity is only two. For simplicity, we only consider such generic exceptional points in this article. Since their algebraic multiplicities are two, they do not admit other generalized eigenfunctions, i.e., the equation

$$L_0 u_{g2} = u_g$$

admits no solutions for u_{g2} in the Hilbert space. Since $\mathcal{P}u_e$ is in the kernel of the adjoint operator $L_0^\dagger$, the Fredholm condition on the above equation is

$$D \equiv \langle u_g, u_e \rangle_{\mathcal{PT}} \neq 0. \tag{4.4}$$

In addition, by taking the $\mathcal{PT}$-product of the equation $L_0 u_g = u_e$ with u_g and recalling the symmetry properties (3.5)–(3.6), we see that D is real.

If the potential $V_0(x)$ is perturbed to be (4.1), we study nonlinear dynamics in this perturbed potential by multiscale perturbation methods. First, we expand the solution to Eq. (2.1) into a perturbation series,

$$\psi(x,z) = \left(\epsilon u_1(x,Z) + \epsilon^2 u_2 + \epsilon^3 u_3 + \cdots\right) \mathrm{e}^{-\mathrm{i}\mu_0 z}, \tag{4.5}$$

which is a slowly-modulated small-amplitude solution. Here $Z = \epsilon z$ is the slow-modulation scale. Then, up to order ϵ^3 we get a system of equations

$$L_0 u_1 = 0,$$
$$L_0 u_2 = -\mathrm{i} u_{1Z},$$
$$L_0 u_3 = -\mathrm{i} u_{2Z} - V_2 u_1 - \sigma |u_1|^2 u_1.$$

Since $\mathcal{P}u_e$ is in the kernel of the adjoint operator $L_0^\dagger$, the solvability conditions for these equations are that their right sides be orthogonal to $\mathcal{P}u_e$.

At orders ϵ and ϵ^2 we find from (4.3) that

$$u_1 = A u_e, \tag{4.6a}$$
$$u_2 = -\mathrm{i} A_Z u_g, \tag{4.6b}$$

where $A(Z)$ is the slowly-varying amplitude function of the eigenmode $u_e(x)$. At order ϵ^3 we have

$$L_0 u_3 = -A_{ZZ} u_g - A V_2 u_e - \sigma |A|^2 A |u_e|^2 u_e.$$

The solvability condition of this equation yields

$$A_{ZZ} - \alpha A + \sigma_1 |A|^2 A = 0, \tag{4.7}$$

where

$$\alpha = -\frac{1}{D}\langle V_2 u_e, u_e \rangle_{\mathcal{PT}}, \qquad \sigma_1 = \frac{\sigma}{D}\langle |u_e|^2 u_e, u_e \rangle_{\mathcal{PT}}. \tag{4.8}$$

Eq. (4.7) for the wave-amplitude function $A(Z)$ is our reduced model for nonlinear wave dynamics near an exceptional (phase-transition) point. Since $V_2(x)$ is $\mathcal{PT}$-symmetric and D real, α and σ_1 are real.

The reduced model (4.7) is a fourth-order dynamical system since A is complex. However it has two conserved quantities,

$$I_1 = |A_Z|^2 - \alpha |A|^2 + \frac{\sigma_1}{2}|A|^4, \tag{4.9}$$

and

$$I_2 = A^* A_Z - A A_Z^*, \tag{4.10}$$

where $dI_k/dZ = 0$ $(k = 1, 2)$. Due to these two conserved quantities, solution dynamics in Eq. (4.7) is confined to a two-dimensional surface, thus this dynamics cannot be chaotic. When $Z \to \infty$, the solution A can only approach a fixed point, or a periodic orbit, or infinity (if $\sigma_1 > 0$, infinity is further forbidden due to the conservation of I_1).

The parameter α plays an important role in Eq. (4.7). Let us consider the small-amplitude limit ($|A| \ll 1$), in which case Eq. (4.7) reduces to $A_{ZZ} - \alpha A = 0$. If $\alpha < 0$, these infinitesimal (linear) modes are bounded, meaning that the system is below phase transition. But, if $\alpha > 0$, these linear modes grow exponentially, indicating that the system is above phase transition. Recall that α is dependent on the potential perturbation V_2. Thus, whether the perturbed potential is above or below phase transition depends on the sign of α. In addition, the value of α also determines whether or not the underlying exceptional point $\mu = \mu_0$ is a phase-transition point: if $\alpha \neq 0$, then $\mu = \mu_0$ is a phase-transition point; if $\alpha = 0$, then the answer is not certain, and further analysis is needed.

In the next two sections, we will describe the predictions of the reduced model (4.7) and compare them with the full system (2.1). In all our numerical comparisons, we will use the Scarff-II potential (2.3) with $V_R = 2$. At this V_R value, an exceptional point occurs when

$$W_0 = 2.25, \qquad \mu_0 \approx -0.3144, \tag{4.11}$$

and this exceptional point is a phase-transition point. In the format (4.1), this Scarff-II potential has

$$V_0(x) = 2\,\mathrm{sech}^2(x) + \mathrm{i}2.25\,\mathrm{sech}(x)\tanh(x), \tag{4.12a}$$
$$V_2(x) = \mathrm{i}c\,\mathrm{sech}(x)\tanh(x). \tag{4.12b}$$

This potential is above phase transition when $c = 1$ and below phase transition when $c = -1$. At this phase-transition point, the coefficients in the reduced model (4.7) are found to be

$$\alpha \approx 0.3144c, \qquad \sigma_1 \approx 0.2700\sigma. \tag{4.13}$$

For these coefficients the eigenfunction $u_e(x)$ has been normalized to have unit amplitude. In all our comparisons, we take $\epsilon = 0.2$. This ϵ is not very small, but predictions of the reduced model (4.7) still match those in the full system (2.1) as we will see below.

5. Solution behaviors above phase transition

Our main interest is to investigate nonlinear wave dynamics above phase transition ($\alpha > 0$). Previous studies on nonlinear $\mathcal{PT}$-symmetric systems overwhelmingly focused on solution behaviors below phase transition, because it was argued that coherent structures such as solitons would be unstable above phase transition (at least in $\mathcal{PT}$-symmetric periodic potentials). We will show in this section that in $\mathcal{PT}$-symmetric localized potentials, stable solitons and robust oscillating nonlinear modes do exist above phase transition.

5.1. Soliton families and their stability

First we consider soliton solutions, which correspond to constant-amplitude solutions in the reduced model (4.7). Specifically, constant-amplitude solutions of the form

$$A(Z) = A_0 \mathrm{e}^{-\mathrm{i}\mu_1 Z} \tag{5.1}$$

in Eq. (4.7) correspond to soliton solutions of the form

$$\psi = u(x)\,\mathrm{e}^{-\mathrm{i}(\mu_0 + \epsilon\mu_1)z} \tag{5.2}$$

in Eq. (2.1), where $u(x) \approx \epsilon A_0 u_e(x)$ to leading order. In this A-formula, A_0 is a constant which will be made real positive from phase invariance. Substituting (5.1) into (4.7), we find μ_1 as

$$\mu_1 = \pm\sqrt{\sigma_1 A_0^2 - \alpha}, \tag{5.3}$$

where the quantity under the square root must be non-negative. This equation relates the propagation constant μ_1 to the soliton amplitude parameter A_0.

Since $\alpha > 0$ above phase transition, solutions (5.3) exist only when $\sigma_1 > 0$. For the Scarff-II potential (4.12), this means that above phase transition, solitons can only exist under self-focusing nonlinearity ($\sigma > 0$). The physical reason for the existence of these solitons comes from the nonlinear feedback. It is commonly known that a $\mathcal{PT}$-symmetric complex potential is above phase transition when the imaginary part of the potential (relative to the real part) is above a certain threshold. In the current case, even though the linear potential $V(x;\epsilon)$ is above phase transition, the effective potential, which is this linear potential plus the nonlinearity-induced positive refractive index $\sigma|\psi|^2$, can still be below phase transition since the real part of this effective potential is enhanced by nonlinearity, which makes the imaginary part of the effective potential relatively weaker. As a consequence, the nonlinearity can transform the effective potential from above phase transition to below phase transition [25,32].

Notice also from Eq. (5.3) that these solitons exist only above a certain amplitude threshold, which is

$$A_0^2 \geq \alpha/\sigma_1. \tag{5.4}$$

This means that the nonlinearity-induced positive refractive index must be strong enough to transform the effective potential from above to below phase transition. Consequently, these solitons do not bifurcate from linear modes of the potential. In addition, the two branches of these solutions (corresponding to the plus and minus signs in (5.3)) are connected at this amplitude threshold and thus belong to a single soliton family.

For the Scarff-II potential (4.1) with (4.12), $c = 1$ and $\epsilon = 0.2$, we have numerically obtained these predicted solitons above phase transition under focusing nonlinearity ($\sigma = 1$). The profile of this complex potential is displayed in Fig. 2(a), and its linear spectrum is shown in Fig. 2(b). This linear spectrum contains a complex-conjugate pair of discrete eigenvalues, indicating that this potential is above phase transition. The power curve of solitons we numerically obtained is plotted in Fig. 2(c). Here the soliton's power is defined as $P(\mu) = \int_{-\infty}^{\infty} |\psi|^2 dx$. It is seen that this numerical power curve indeed has a minimum threshold. The analytical prediction for this power threshold, obtained from Eq. (5.4) and the leading-order perturbation solution (4.5) as

$$P_{\min} = \frac{\alpha\epsilon^2}{\sigma_1} \int_{-\infty}^{\infty} |u_e|^2 dx,$$

is also depicted in Fig. 2(c) (as a horizontal dashed line). It is seen that this analytical power threshold matches the numerical value very well. At the black-dot point of the numerical power curve (where $\mu = -0.5$), the profile of the corresponding soliton solution is illustrated in Fig. 2(d). This soliton is $\mathcal{PT}$-symmetric, as are all other solitons in this family.

Stability of these solitons can be analyzed by examining the stability of constant-amplitude solutions (5.1) in the reduced ODE model (4.7). Let us perturb this constant-amplitude solution by normal modes as

$$A(Z) = \left(A_0 + \widetilde{A}\, e^{\lambda_A Z} + \widetilde{B}^* e^{\lambda_A^* Z}\right) e^{-i\mu_1 Z},$$

where $\widetilde{A}, \widetilde{B} \ll 1$, and λ_A is the eigenvalue from the ODE model. Plugging this into (4.7) and linearizing, we obtain

$$L_A \begin{pmatrix} \widetilde{A} \\ \widetilde{B} \end{pmatrix} = 0,$$

where

$$L_A = \begin{pmatrix} \lambda_A^2 - 2i\lambda_A\mu_1 + \mu_1^2 + \alpha & \mu_1^2 + \alpha \\ \mu_1^2 + \alpha & \lambda_A^2 + 2i\lambda_A\mu_1 + \mu_1^2 + \alpha \end{pmatrix}.$$

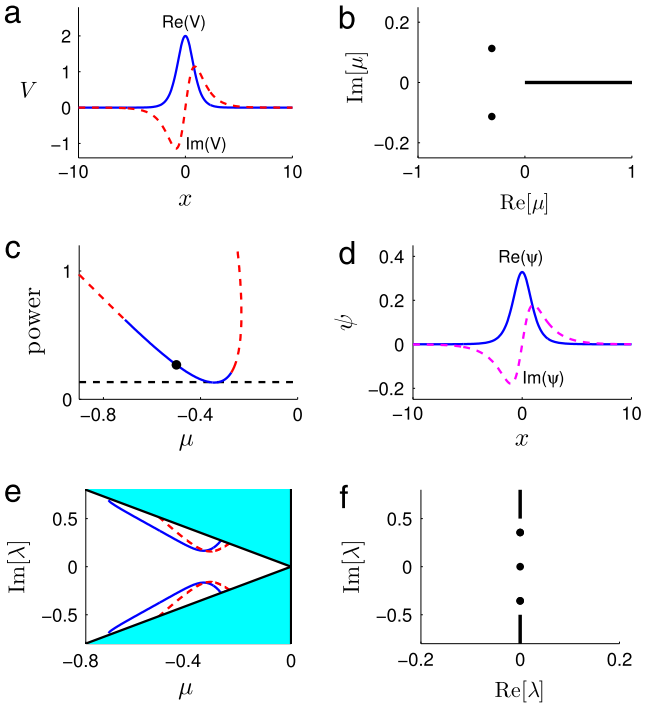

Fig. 2. (a) Profile of the Scarff-II potential (4.1), (4.12) with $c = 1$ and $\epsilon = 0.2$; (b) linear spectrum of this Scarff-II potential in (a), which shows that this potential is above phase transition; (c) power curve for the family of solitons in this Scarff-II potential under focusing nonlinearity ($\sigma = 1$); solid blue indicates stable solitons and dashed red unstable ones; the horizontal dashed line is the analytical prediction for the power minimum; (d) profile of an example soliton at the black-dot point of the power curve (where $\mu = -0.5$); (e) discrete eigenvalues for stable solitons versus the propagation constant μ; solid blue are numerical values and dashed red analytical predictions; the shaded region is the continuous spectrum; (f) the numerically obtained linear-stability spectrum for the soliton in panel (d). (For interpretation of the references to color in this figure legend, the reader is referred to the web version of this article.)

Requiring the determinant of this matrix L_A to vanish, non-zero eigenvalues λ_A are then derived as

$$\lambda_A = \pm i\sqrt{2(3\mu_1^2 + \alpha)}.$$

Since $\alpha > 0$ above phase transition, this formula predicts a pair of purely imaginary discrete eigenvalues, indicating that the constant-amplitude solution (5.1) is linearly stable in the ODE model (4.7). This suggests that the soliton solution (5.2) is also linearly stable in the original system (2.1). Taking into account the scaling $Z = \epsilon z$, an approximation for non-zero discrete eigenvalues of this soliton is

$$\lambda \approx \epsilon\lambda_A = \pm i\epsilon\sqrt{2(3\mu_1^2 + \alpha)}. \tag{5.5}$$

Numerically we have confirmed the linear stability of these solitons near phase transition. This is achieved by computing the linear-stability spectrum of these solitons by the Fourier-collocation method [43]. The reader is reminded that this linear-stability problem for solitons is different from that for the zero state considered in Section 3. As an example, for the soliton shown in Fig. 2(d), its linear-stability spectrum is displayed in Fig. 2(f). All eigenvalues in this spectrum are purely imaginary, indicating that the soliton is linearly stable. In addition, the pair of discrete imaginary eigenvalues in this spectrum correspond to those predicted by formula (5.5). Similar computations are performed for other solitons, and their stability is indicated by solid blue lines on the power diagram of Fig. 2(c). It is interesting to note that solitons on both sides of the power minimum (with opposite signs of power slopes) are linearly stable. This contrasts the case in many

conservative systems, where a sign change in power slope signals a switching of linear stability [43]. The reason for non-switching of linear stability here is that, the theorems predicting stability switching at a power extremum (such as the Vakhitov–Kolokolov criterion and others) do not apply to the present non-conservative system [43]. More specifically, a stability-switching criterion for $\mathcal{PT}$-symmetric solitons in Eq. (2.1) was derived in [19]. For real potentials (the conservative case), this criterion predicts stability switching at a power extremum, in agreement with the previous theory. However, for complex potentials, this criterion predicts that stability switching of $\mathcal{PT}$ solitons does not occur at a power extremum in general, and Fig. 2(c) is another numerical example corroborating this prediction. Quantitative comparison between numerical discrete imaginary eigenvalues and their analytical prediction (5.5) is made in Fig. 2(e), and reasonable agreement can be seen (even though $\epsilon = 0.2$ is not small here).

At higher power values, we find that these solitons become linearly unstable, and this instability is shown by dashed red lines on the power curve of Fig. 2(c). The instability on the left side of the power curve is induced by a collision between the discrete imaginary eigenvalue shown in Fig. 2(e), (f) and another discrete imaginary eigenvalue bifurcated out of the edge of the continuous spectrum. This collision occurs at $\lambda \approx \pm 0.690i$ on the imaginary axis (near the edges of the continuous spectrum) when $\mu \approx -0.711$, and it creates a quartet of complex eigenvalues bifurcating off the imaginary axis (analogous to a Hamiltonian–Hopf bifurcation). The instability on the right side of the power curve, on the other hand, is caused by a collision between the discrete imaginary eigenvalue shown in Fig. 2(e), (f) and the edge of the continuous spectrum. This collision occurs when $\mu \approx -0.273$ (on the right side of the power minimum point), and it creates a quartet of complex eigenvalues bifurcating off the edges of the continuous spectrum.

5.2. Oscillating solutions

The behavior of solutions away from the soliton equilibria can be largely captured by focusing on the case where A is purely real in the reduced model (4.7). In this case, the model equation becomes a simple second-order ODE which we analyze using phase portraits. Above phase transition ($\alpha > 0$), this breaks into two cases depending on the sign of the nonlinearity.

5.2.1. Positive σ_1

In this case, the phase portrait is shown in Fig. 3(a), where α and σ_1 values are taken from Eq. (4.13) with $c = 1$ and $\sigma = 1$ (focusing nonlinearity). This phase portrait contains three fixed points. One of them is the origin, which is unstable, signifying that the system is above phase transition. The other two fixed points are at $A = \pm\sqrt{\alpha/\sigma_1}$, which are stable, and they correspond to the soliton of minimum power (with $\mu_1 = 0$) in Eqs. (5.3)–(5.4). Away from these fixed points, the phase portrait features two types of periodic orbits which are separated by a figure-eight trajectory joined at the origin. Inner periodic orbits surround the non-zero fixed points, while outer periodic orbits undergo wider amplitude swings.

These periodic orbits in the phase plane imply the existence of robust oscillating solutions away from solitons in the full system (2.1), and such oscillating solutions are confirmed in our direct evolution simulations of that system. To illustrate, two examples of such PDE solutions are displayed in Fig. 3(b), (c). Oscillations in panel (b) are stronger, and they correspond to outer periodic orbits in the phase portrait (a). Oscillations in panel (c) are weaker, and they correspond to inner periodic orbits in the phase portrait. This solution correspondence can be made more explicit by projecting

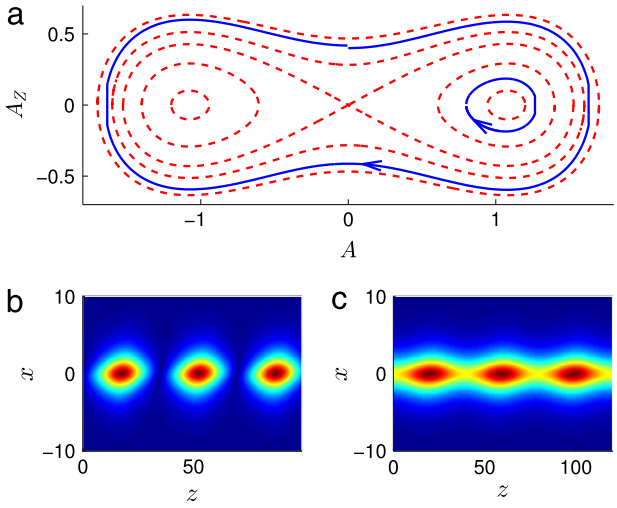

Fig. 3. (a) Phase portrait of the reduced model (4.7) with $\sigma_1 > 0$ above phase transition. (b, c) Full PDE simulations in the Scarff-II potential (4.12) with $\sigma = 1$, $c = 1$ and $\epsilon = 0.2$ under different initial conditions. In (a), solid blue lines are full PDE solutions in (b, c) projected onto the phase plane (with the outer curve for (b) and inner curve for (c)). (For interpretation of the references to color in this figure legend, the reader is referred to the web version of this article.)

the PDE solution onto the phase plane. To do so, we recall the perturbation solution (4.5)–(4.6), which to order ϵ^2 gives

$$\psi(x,z) = \left[\epsilon A(Z)u_e(x) - \mathrm{i}\epsilon^2 A'(Z)u_g(x)\right]\mathrm{e}^{-\mathrm{i}\mu_0 z}. \tag{5.6}$$

Taking the $\mathcal{PT}$-product of this equation with $u_g(x)$ and retaining only the leading-order term, we get

$$A(Z) = \frac{\langle u_g, \psi(x, Z/\epsilon)\rangle_{\mathcal{PT}}}{\epsilon D}\,\mathrm{e}^{\mathrm{i}\mu_0 Z/\epsilon}. \tag{5.7}$$

Taking the $\mathcal{PT}$-product of (5.6) with $u_e(x)$ and recalling that $\langle u_e, u_e\rangle_{\mathcal{PT}} = 0$, we get

$$A'(Z) = \frac{\mathrm{i}\langle u_e, \psi(x, Z/\epsilon)\rangle_{\mathcal{PT}}}{\epsilon^2 D}\,\mathrm{e}^{\mathrm{i}\mu_0 Z/\epsilon}. \tag{5.8}$$

In this way, the full PDE solution can be embedded in the phase portrait of the ODE model for comparison. As a technical matter, the projected quantities (A, A') from the PDE solution by (5.7)–(5.8) are complex in general. But we have found that if the initial condition of the PDE solution is chosen according to Eq. (5.6), then the imaginary parts of the projected (A, A') remain very small for very long distances. Thus we neglect those small imaginary parts and plot only the real parts of the projected (A, A') in the phase plane.

For the two PDE solutions in Fig. 3(b), (c), their phase-plane projections are displayed as solid blue lines in panel (a). It is seen that these PDE projections closely mimic the periodic orbits of the ODE model.

It is noted that these predictions of periodically-oscillating solutions in the PDE system are valid on the distance scale of $z \sim 1/\epsilon$. Beyond this distance scale, the PDE dynamics generally starts to deviate from the ODE predictions. Our numerics show that over very long distances, these oscillations in the PDE solution gradually intensify and eventually break up. This phenomenon resembles that of solitons in Hamiltonian systems with internal modes of negative Krein signatures or with Hamiltonian–Hopf bifurcations [44,45].

5.2.2. Negative σ_1

When $\sigma_1 < 0$, the phase portrait is shown in Fig. 4 (left panel), where α and σ_1 values are taken from Eq. (4.13) with $c = 1$ and $\sigma = -1$ (defocusing nonlinearity). In this case, except for the

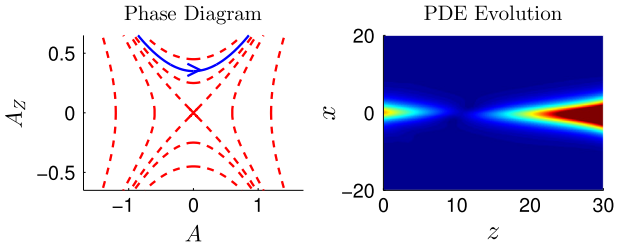

Fig. 4. (Left) Phase portrait of the reduced model (4.7) with $\sigma_1 < 0$ above phase transition. (Right) Full PDE simulation in the Scarff-II potential (4.12) with $\sigma = -1$, $c = 1$ and $\epsilon = 0.2$. The solid blue line in the left panel is this full PDE solution projected onto the phase plane. (For interpretation of the references to color in this figure legend, the reader is referred to the web version of this article.)

origin (an unstable fixed point), all trajectories escape to infinity. Similar solution behaviors are observed in the full PDE (2.1). An example is shown in the right panel of Fig. 4, where the PDE solution is seen to first decrease, and then rise to higher amplitudes. The projection of this PDE solution onto the phase plane is displayed as a solid blue line in the phase portrait. This projection closely follows the trajectory of the ODE model. After the solution amplitude has risen to the order of $\epsilon A \sim O(1)$ (beyond the validity of our perturbation theory), the PDE solution eventually saturates in amplitude while continuing to emit radiation and growing in power. As $z \to \infty$, the amplitude $|u(x, z)|$ of the PDE solution approaches an asymmetric stationary state with constant shelves at large distances ($|x| \gg 1$), and this stationary state attracts almost all nonzero localized initial conditions.

6. Solution behaviors below phase transition

In this section, we consider the predictions of our reduced model for solution behaviors below phase transition, and compare them with PDE solutions.

6.1. Soliton solutions

Below phase transition ($\alpha < 0$), the ODE model (4.7) admits constant-amplitude solutions (5.1) for both signs of the nonlinear coefficient σ_1, meaning that solitons exist under both focusing and defocusing nonlinearities. But behaviors of solitons for the two signs of σ_1 are very different.

When $\sigma_1 > 0$, formula (5.3), when rewritten as

$$A_0^2 = (\mu_1^2 + \alpha)/\sigma_1, \tag{6.1}$$

predicts that constant-amplitude solutions exist when $|\mu_1| > \sqrt{|\alpha|}$, i.e., soliton solutions exist when $|\mu - \mu_0| > \epsilon\sqrt{|\alpha|}$. In addition, the amplitude A_0 (and hence power) of these solitons can be arbitrary. Numerically we have confirmed this prediction in the Scarff-II potential (4.12) with $\sigma = 1$, $c = -1$ and $\epsilon = 0.2$. The numerically obtained power curves of these solitons are displayed in Fig. 5(a).

Stability of these solitons may be analyzed in the framework of the reduced model (4.7). The eigenvalue formula (5.5) shows that these eigenvalues are purely imaginary since $3\mu_1^2 + \alpha > \mu_1^2 + \alpha > 0$ here. This suggests that these solitons are linearly stable at low amplitudes (where the perturbation theory is valid). This prediction proves to be correct for the left branch of the soliton family, which is numerically found to be linearly stable at low amplitudes, see Fig. 5(a) (at higher amplitudes, they become unstable due to a quartet of complex eigenvalues bifurcating off the edges of the continuous spectrum at $\mu \approx -0.75$ when a pair of purely imaginary discrete eigenvalues collide with these edges). The right branch of the soliton family, however, is all linearly unstable, in disagreement with the ODE model's prediction. This

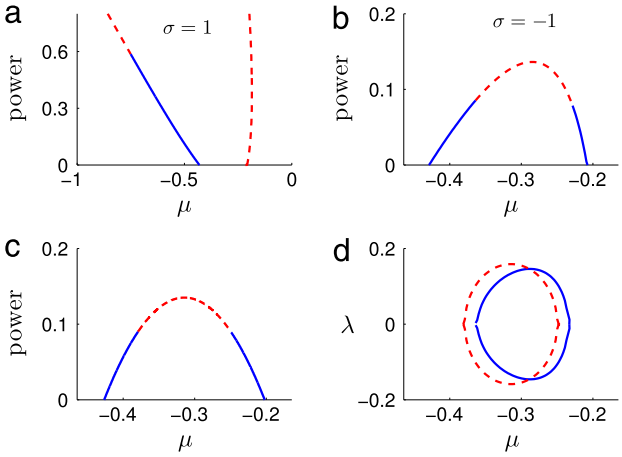

Fig. 5. (a,b) Numerically obtained power curves for the families of solitons below phase transition in the Scarff-II potential (4.12) with $c = -1, \epsilon = 0.2, \sigma = 1$ in (a) and $\sigma = -1$ in (b). (c) Analytical prediction for the power curve and linear stability of solitons in (b). In all of (a, b, c), solid blue indicates stable solitons and dashed red unstable ones. (d) Comparison of numerically obtained (solid blue) and analytically predicted (dashed red) unstable eigenvalues for solitons in (b). (For interpretation of the references to color in this figure legend, the reader is referred to the web version of this article.)

linear instability in solitons of the right branch is due to a quartet of complex eigenvalues, which bifurcate out from a pair of embedded eigenvalues inside the continuous spectrum when the solitons bifurcate out from the zero-amplitude limit. This pair of embedded eigenvalues at the zero-amplitude limit is located at $\pm i\,(\mu_2 - \mu_1)$, where $\mu_1 \approx -0.4303$ and $\mu_2 \approx -0.2079$ are the two discrete eigenvalues of the linear $\mathcal{PT}$ potential. These eigenvalues are embedded inside the continuous spectrum of $\pm i\,[|\mu_2|, \infty)$ and bifurcate off the imaginary axis when the solitons bifurcate out. We note that while the reduced model misses this eigenvalue bifurcation into the complex plane, it does successfully predict the embedded eigenvalues where this bifurcation occurs. Specifically, at the zero-amplitude limit ($A_0 = 0$), the ODE model predicts $\mu = \mu_0 + \epsilon\sqrt{|\alpha|}$, hence the continuous spectrum is located at $\pm i\,[|\mu|, \infty)$, but the discrete eigenvalues (5.5) are at $\lambda = \pm 2i\epsilon\sqrt{|\alpha|}$, which are embedded inside this continuous spectrum for the underlying μ_0, ϵ and α values.

When $\sigma_1 < 0$, formulae (5.3) and (6.1) predict that solitons only exist in the propagation-constant interval of $|\mu - \mu_0| < \epsilon\sqrt{|\alpha|}$ with a limited range of amplitude values $|A_0| \leq \sqrt{\alpha/\sigma_1}$. The analytically predicted power curve from Eqs. (4.5), (4.6) and (6.1) is

$$P(\mu) \approx \frac{(\mu - \mu_0)^2 + \alpha\epsilon^2}{\sigma_1} \int_{-\infty}^{\infty} |u_e|^2 dx, \tag{6.2}$$

which is plotted in Fig. 5(c). Numerically we have obtained these solitons, whose power curve is shown in Fig. 5(b). This numerical power curve closely resembles the analytical prediction in (c). In particular, the existence of a power upper bound is confirmed. This close agreement between the perturbation theory and direct numerics is understandable, since these solitons have low powers and are thus within the regime of validity of the perturbation theory.

The physical reason for limited power ranges of these solitons is that, under defocusing nonlinearity, if this power is too high, the negative nonlinearity-induced refractive index would transform the effective potential from below phase transition to above phase transition, rendering stationary solitons impossible.

Stability of these solitons with limited power ranges can be analyzed in the framework of the reduced model (4.7). In this

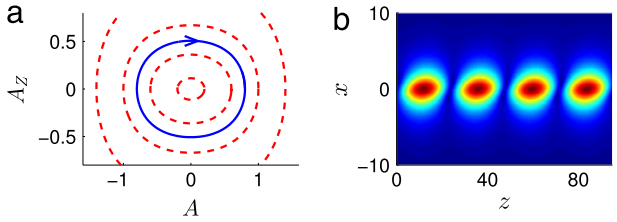

Fig. 6. (Left) Phase portrait of the reduced model (4.7) with $\sigma_1 > 0$ below phase transition. (Right) Full PDE simulation in the Scarff-II potential (4.12) with $\sigma = 1$, $c = -1$ and $\epsilon = 0.2$. The solid blue line in the left panel is this full PDE solution projected onto the phase plane. (For interpretation of the references to color in this figure legend, the reader is referred to the web version of this article.)

case, the eigenvalue formula (5.5) predicts that these solitons are linearly unstable when

$$|\mu - \mu_0| < \epsilon\sqrt{|\alpha|/3}, \tag{6.3}$$

and stable otherwise. This predicted instability and stability are shown in the predicted power curve in Fig. 5(c). It is seen that solitons at the top part of the power curve are predicted as unstable and the bottom ones predicted as stable. Numerically we have determined the linear stability of these solitons by computing their stability spectra, and the results are shown in Fig. 5(b). Clearly the numerical results match those of analytical predictions. Quantitatively we have also computed real eigenvalues of unstable solitons and plotted them in Fig. 5(d), together with their analytical predictions in Eq. (5.5). This quantitative comparison shows good agreement as well. The good agreement on the instability here is due to the fact that this instability is caused by real eigenvalues, which can be captured by the underlying perturbation theory.

6.2. Oscillating solutions

Like the previous case above phase transition, robust oscillating solutions exist below phase transition as well. As before, we will unveil such solutions by focusing on the case of real A in the reduced model (4.7).

If $\sigma_1 > 0$, the phase portrait of the reduced model is shown in Fig. 6 (left panel), where α and σ_1 values are taken from Eq. (4.13) with $c = -1$ and $\sigma = 1$ (focusing nonlinearity). In this phase portrait the origin is a stable fixed point, a reflection that the system is below phase transition. Surrounding the origin are periodic orbits of various sizes. This implies an abundance of robust oscillating solutions in the PDE system. Numerically we have confirmed the existence of these oscillating solutions, and an example is shown in Fig. 6 (right panel). Projection of this PDE solution onto the phase plane is plotted as a solid blue line in the left panel, and good agreement with the ODE orbit is seen.

If $\sigma_1 < 0$, the phase portrait of the reduced model (4.7) is shown in Fig. 7(a), where α and σ_1 values are taken from Eq. (4.13) with $c = -1$ and $\sigma = -1$ (defocusing nonlinearity). This phase portrait contains three fixed points: the origin which is stable, and $A = \pm\sqrt{\alpha/\sigma_1}$ which are unstable. The latter two fixed points correspond to the soliton with maximal power (at $\mu = \mu_0$) in Fig. 5(c). Away from these three equilibria, trajectories are divided into two categories: periodic orbits surrounding the origin, and orbits which escape to infinity. Numerically we have found both types of solutions in the PDE system (2.1) under the Scarff-II potential (4.12) with $\sigma = -1$, $c = -1$ and $\epsilon = 0.2$, and two examples are displayed in Fig. 7(b), (c). Projections of the PDE solutions onto the phase plane in panel (a) indicate that the ODE model accurately describes the PDE dynamics.

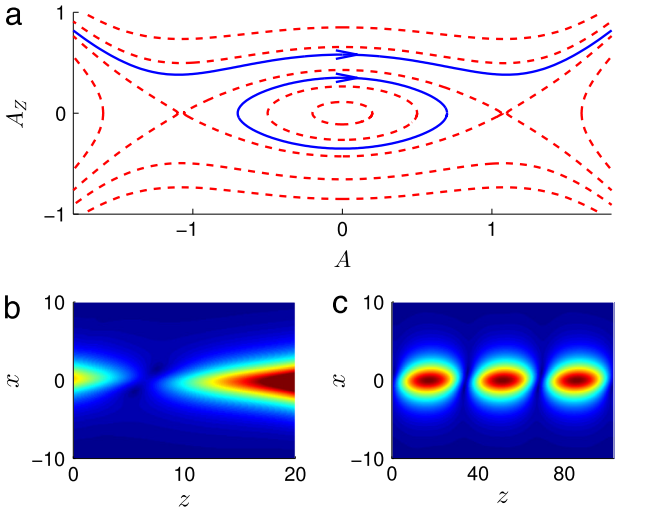

Fig. 7. (a) Phase portrait of the reduced model (4.7) with $\sigma_1 < 0$ below phase transition. (b, c) Full PDE simulations in the Scarff-II potential (4.12) with $\sigma = -1$, $c = -1$ and $\epsilon = 0.2$ under different initial conditions. In (a), solid blue lines are full PDE solutions in (b, c) projected onto the phase plane (with the upper curve for (b) and lower curve for (c)). (For interpretation of the references to color in this figure legend, the reader is referred to the web version of this article.)

7. Summary and discussion

In this article, nonlinear wave propagation in $\mathcal{PT}$-symmetric localized potentials was investigated analytically near a phase transition. Necessary conditions for a phase transition were first derived based on a generalization of the Krein signature. Then rich nonlinear dynamics near a phase transition was revealed through a multi-scale perturbation analysis, which yielded a nonlinear ODE model for the amplitude of the solutions. Above phase transition, this ODE model predicted a family of stable solitons not bifurcating from linear modes under a certain sign of nonlinearity. In addition, it predicted persistent periodically-oscillating solutions away from solitons. Under the opposite sign of nonlinearity, it predicted unbounded growth of solutions. Below phase transition, solution dynamics was predicted as well. We have compared all analytical predictions with direct numerical calculations of the full PDE system and good agreement was obtained.

The analytical results obtained in this article are helpful for several reasons. First, it is known that a phase transition is a distinct and important phenomenon in $\mathcal{PT}$-symmetric systems. Thus the analytical condition for a phase transition in terms of $\mathcal{PT}$-Krein signatures helps understand when a phase transition can or cannot occur. Second, the analytical predictions of nonlinear dynamics near a phase transition contribute to a global understanding of solution behaviors in $\mathcal{PT}$-symmetric systems. Thirdly, even though our analysis was performed only for the potential NLS equation (2.1), a similar treatment can be extended to other $\mathcal{PT}$-symmetric systems near a phase transition, and similar solution dynamics are expected in all such systems.

Along the lines of this work, various extensions can be anticipated. One is the development of $\mathcal{PT}$-Krein signature theory for linear stability of solitons (rather than the zero state) in $\mathcal{PT}$-symmetric systems. Such a theory can help decide when purely-imaginary linear-stability eigenvalues of solitons can bifurcate off the imaginary axis upon collision, creating linear instability and Hopf bifurcations. Another extension is the analysis of solution dynamics near such a Hopf bifurcation in $\mathcal{PT}$-symmetric solitons. At the Hopf bifurcation point, collided purely-imaginary eigenvalues are also exceptional points with non-diagonal Jordan blocks. Thus solution dynamics around such exceptional points may be analyzed by a technique similar to that developed in this article.

Acknowledgments

We thank two anonymous referees for many suggestions which helped improve the presentation of our results. This work was supported in part by the Air Force Office of Scientific Research (USAF 9550-12-1-0244) and the National Science Foundation (DMS-1311730).

References

[1] C.M. Bender, S. Boettcher, Real spectra in non-Hermitian Hamiltonians having $\mathcal{PT}$ symmetry, Phys. Rev. Lett. 80 (1998) 5243–5246.
[2] A. Ruschhaupt, F. Delgado, J.G. Muga, Physical realization of $\mathcal{PT}$-symmetric potential scattering in a planar slab waveguide, J. Phys. A 38 (2005) L171.
[3] R. El-Ganainy, K.G. Makris, D.N. Christodoulides, Z.H. Musslimani, Theory of coupled optical $\mathcal{PT}$-symmetric structures, Opt. Lett. 32 (2007) 2632–2634.
[4] A. Guo, G.J. Salamo, D. Duchesne, R. Morandotti, M. Volatier-Ravat, V. Aimez, G.A. Siviloglou, D.N. Christodoulides, Observation of $\mathcal{PT}$-symmetry breaking in complex optical potentials, Phys. Rev. Lett. 103 (2009) 093902.
[5] C.E. Rueter, K.G. Makris, R. El-Ganainy, D.N. Christodoulides, M. Segev, D. Kip, Observation of parity-time symmetry in optics, Nat. Phys. 6 (2010) 192–195.
[6] A. Regensburger, C. Bersch, M.A. Miri, G. Onishchukov, D.N. Christodoulides, U. Peschel, Parity-time synthetic photonic lattices, Nature 488 (2012) 167–171.
[7] R. Driben, B.A. Malomed, Stability of solitons in parity-time-symmetric couplers, Opt. Lett. 36 (2011) 4323.
[8] J. Schindler, A. Li, M.C. Zheng, F.M. Ellis, T. Kottos, Experimental study of active LRC circuits with $\mathcal{PT}$ symmetries, Phys. Rev. A 84 (2011) 040101(R).
[9] S. Klaiman, U. Günther, N. Moiseyev, Visualization of branch points in $\mathcal{PT}$-symmetric waveguides, Phys. Rev. Lett. 101 (2008) 080402.
[10] H. Cartarius, G. Wunner, Model of a $\mathcal{PT}$-symmetric Bose–Einstein condensate in a δ-function double-well potential, Phys. Rev. A 86 (2012) 013612.
[11] E.M. Graefe, Stationary states of a $\mathcal{PT}$-symmetric two-mode Bose–Einstein condensate, J. Phys. A 45 (2012) 444015.
[12] L. Feng, Y.L. Xu, W.S. Fegadolli, M.H. Lu, J.E.B. Oliveira, V.R. Almeida, Y.F. Chen, A. Scherer, Experimental demonstration of a unidirectional reflectionless parity-time metamaterial at optical frequencies, Nature Mater. 12 (2013) 108–113.
[13] C.M. Bender, B. Berntson, D. Parker, E. Samuel, Observation of $\mathcal{PT}$ phase transition in a simple mechanical system, Amer. J. Phys. 81 (2013) 173179.
[14] B. Peng, S. Özdemir, F. Lei, F. Monifi, M. Gianfreda, G. Long, S. Fan, F. Nori, C.M. Bender, L. Yang, Parity-time-symmetric whispering-gallery microcavities, Nat. Phys. 10 (2014) 394.
[15] L. Feng, Z.J. Wong, R. Ma, Y. Wang, X. Zhang, Single-mode laser by parity-time symmetry breaking, Science 346 (2014) 972–975.
[16] H. Hodaei, M.-A. Miri, M. Heinrich, D.N. Christodoulides, M. Khajavikhan, Parity-time-symmetric microring lasers, Science 346 (2014) 975–978.
[17] Z. Ahmed, Real and complex discrete eigenvalues in an exactly solvable one-dimensional complex $\mathcal{PT}$-invariant potential, Phys. Lett. A 282 (2001) 343.
[18] Z.H. Musslimani, K.G. Makris, R. El-Ganainy, D.N. Christodoulides, Optical solitons in $\mathcal{PT}$-periodic potentials, Phys. Rev. Lett. 100 (2008) 030402.
[19] S. Nixon, L. Ge, J. Yang, Stability analysis for solitons in $\mathcal{PT}$-symmetric optical lattices, Phys. Rev. A 85 (2012) 023822.
[20] F.K. Abdullaev, Y.V. Kartashov, V.V. Konotop, D.A. Zezyulin, Solitons in $\mathcal{PT}$-symmetric nonlinear lattices, Phys. Rev. A 83 (2011) 041805.
[21] M. Miri, A.B. Aceves, T. Kottos, V. Kovanis, D.N. Christodoulides, Bragg solitons in nonlinear $\mathcal{PT}$-symmetric periodic potentials, Phys. Rev. A 86 (2012) 033801.
[22] I.V. Barashenkov, S.V. Suchkov, A.A. Sukhorukov, S.V. Dmitriev, Y.S. Kivshar, Breathers in $\mathcal{PT}$-symmetric optical couplers, Phys. Rev. A 86 (2012) 053809.
[23] D.A. Zezyulin, V.V. Konotop, Nonlinear modes in finite-dimensional $\mathcal{PT}$-symmetric systems, Phys. Rev. Lett. 108 (2012) 213906.
[24] P.G. Kevrekidis, D.E. Pelinovsky, D.Y. Tyugin, Nonlinear stationary states in $\mathcal{PT}$-symmetric lattices, SIAM J. Appl. Dyn. Syst. 12 (2013) 1210.
[25] Y. Lumer, Y. Plotnik, M.C. Rechtsman, M. Segev, Nonlinearly induced $\mathcal{PT}$ transition in photonic systems, Phys. Rev. Lett. 111 (2013) 263901.
[26] J. Yang, Symmetry breaking of solitons in one-dimensional parity-time-symmetric optical potentials, Opt. Lett. 39 (2014) 5547–5550.
[27] S.V. Suchkov, A.A. Sukhorukov, J. Huang, S.V. Dmitriev, C. Lee, Y.S. Kivshar, Nonlinear switching and solitons in $\mathcal{PT}$-symmetric photonic systems, 2015. arXiv:1509.03378 [physics.optics].
[28] V.V. Konotop, J. Yang, D.A. Zezyulin, Nonlinear waves in $\mathcal{PT}$-symmetric systems, 2016. arXiv:1603.06826 [nlin.PS].
[29] Z. Lin, H. Ramezani, T. Eichelkraut, T. Kottos, H. Cao, D.N. Christodoulides, Unidirectional invisibility induced by $\mathcal{PT}$-symmetric periodic structures, Phys. Rev. Lett. 106 (2011) 213901.
[30] S. Nixon, Y. Zhu, J. Yang, Nonlinear dynamics of wave packets in $\mathcal{PT}$-symmetric optical lattices near the phase transition point, Opt. Lett. 37 (2012) 4874–4876.
[31] S. Nixon, J. Yang, Pyramid diffraction in parity-time-symmetric optical lattices, Opt. Lett. 38 (2013) 1933–1935.
[32] I.V. Barashenkov, D.E. Pelinovsky, P. Dubard, Dimer with gain and loss: Integrability and $\mathcal{PT}$-symmetry restoration, J. Phys. A 48 (2015) 325201.
[33] M. Nazari, F. Nazari, M.K. Moravvej-Farshi, Dynamic behavior of spatial solitons propagating along Scarf II parity-time symmetric cells, J. Opt. Soc. Amer. B 29 (2012) 3057–3062.
[34] Z. Shi, X. Jiang, X. Zhu, H. Li, Bright spatial solitons in defocusing Kerr media with $\mathcal{PT}$-symmetric potentials, Phys. Rev. A 84 (2011) 053855.
[35] H. Chen, S. Hu, L. Qi, The optical solitons in the Scarff parity-time symmetric potentials, Opt. Commun. 331 (2014) 139.
[36] R.S. MacKay, Stability of equilibria of Hamiltonian systems, in: R.S. MacKay, J. Meiss (Eds.), Hamiltonian Dynamical Systems, Adam Hilger, Bristol, 1987, pp. 137–153.
[37] D.E. Pelinovsky, Localization in Periodic Potentials: From Schrödinger Operators to the Gross–Pitaevskii Equation, Cambridge University Press, Cambridge, UK, 2011.
[38] T. Kapitula, K. Promislow, Spectral and Dynamical Stability of Nonlinear Waves, Springer, New York, 2013.
[39] R. Kollar, R.L. Pego, Spectral stability of vortices in two-dimensional Bose–Einstein condensates via the Evans function and Krein signature, Appl. Math. Res. Express 2012 (2012) 1–46.
[40] A. Mostafazadeh, Pseudo-Hermitian representation of quantum mechanics, Int. J. Geom. Methods Mod. Phys. 7 (2010) 1191–1306.
[41] C.M. Bender, D.C. Brody, H.F. Jones, Complex extension of quantum mechanics, Phys. Rev. Lett. 89 (2002) 270401.
[42] R. Kollar, P.D. Miller, Graphical Krein signature theory and Evans–Krein functions, SIAM Rev. 56 (2014) 73–123.
[43] J. Yang, Nonlinear Waves in Integrable and Nonintegrable Systems, SIAM, Philadelphia, 2010.
[44] P.G. Kevrekidis, D.E. Pelinovsky, A. Saxena, When linear stability does not exclude nonlinear instability, Phys. Rev. Lett. 114 (2015) 214101.
[45] J. Yang, A normal form for Hamiltonian–Hopf bifurcations in generalized nonlinear Schrodinger equations, SIAM J. Appl. Math. 76 (2016) 598–617.